Journal of Hydrology 598 (2021) 126419

Contents lists available at ScienceDirect

Journal of Hydrology

journal homepage: www.elsevier.com/locate/jhydrol

Research papers

Links between global terrestrial water storage and large-scale modes of climatic variability

Lanlan Guo [a,b], Tiewei Li [b], Deliang Chen [c], Junguo Liu [d], Bin He [e,*], Yafeng Zhang [e]

[a] State Key Laboratory of Earth Surface Processes and Resource Ecology, Beijing Normal University, Beijing 100875, PR China
[b] Faculty of Geographical Science, Beijing Normal University, Beijing 100875, PR China
[c] Regional Climate Group, Department of Earth Sciences, University of Gothenburg, Sweden
[d] School of Environmental Science and Engineering, Southern University of Science and Technology, Shenzhen 518055, PR China
[e] College of Global Change and Earth System Science, Beijing Normal University, Beijing 100875, PR China

ARTICLE INFO

This manuscript was handled by Marco Borga, Editor-in-Chief, with the assistance of Yadu Pokhrel, Associate Editor

Keywords:
Terrestrial water storage
Teleconnections
Evapotranspiration
Precipitation
Runoff

ABSTRACT

Large-scale states of ocean and atmosphere control the quantity and routine of vapor transported into land and the land water storage pattern. However, the contributions of leading climatic modes, or teleconnections (TCs), to global terrestrial water storage (TWS) variations are poorly understood. Here, we use measurements from the Gravity Recovery and Climate Experiment (GRACE) satellite mission to study 14 main TC controls on river basins and continental and global water storage patterns. Variations in terrestrial water storage anomaly (TWSA) in>97.5% of the global land surface are significantly correlated with at least 1 studied climatic mode. Among the 14 leading climatic modes, the El Niño-Southern Oscillation (ENSO), Pacific Decadal Oscillation (PDO), Atlantic Multidecadal Oscillation (AMO), and Indian Ocean Dipole (IOD) affect terrestrial water storage in 76.5%, 74.6%, 59.7% and 46.4% of the global land surface, respectively. By associating each TC contribution, ENSO appears to have a weaker control on global land water storage than previously thought for dominating TWSA in 31.8% of global land, in contrast to PDO dominating TWSA in 36.6%. Our results suggest that the phase combination of TCs adjusts the response degree and time lag of land water storage via different hydrological cycle components, while the processes remain dynamic and highly uncertain.

1. Introduction

Large-scale and periodic changes in the single or coupled states of the ocean and atmosphere, usually expressed as teleconnections (TCs) for driving Earth climate remotely, are expected to regulate the general dynamics of the terrestrial hydrological cycle (Hallett et al., 2004; Martens et al., 2018). For example, the El Niño–Southern Oscillation (ENSO), as a key mode of variability in global atmospheric circulation, is associated with large-scale fluctuations in precipitation patterns and ultimately influences terrestrial water inputs (Forootan et al., 2014; Sun et al., 2016; Emerton et al., 2017). It also shifts atmospheric and ecological water demands via temperature and radiation fluctuations, subsequently altering the global terrestrial evapotranspiration and adjusting the output flux of terrestrial water resource (Miralles et al., 2014; Feng et al., 2018; Martens et al, 2018). Beyond the water budget, the buffering and reallocation processes of water among terrestrial water bodies (e.g., rivers, lakes) and ecosystems (e.g., plants, soil) are likewise regulated by certain identified climatic modes (Long et al., 2014; Emerton et al., 2017; McGregor, 2017). Terrestrial water storage (TWS) links energy and moisture exchanges between the atmosphere, ocean, and ecosystem and translates remote signals of hydrological elements that the atmosphere and ocean bring with them (De Linage et al., 2013; Forootan et al., 2016).

Terrestrial water supports ecosystems and human society. The interannual fluctuations in land water storage strongly affect the terrestrial carbon sink at global to regional scales (Fang et al., 2017; Humphrey et al., 2018). It is critical to disentangle the effects of climatic modes and improve the global water resource forecasting ability under climate change. Based upon the current theoretical understanding and instrumental observation of climatic teleconnections, several studies have revealed that ENSO is strongly correlated with the interannual changes in TWS between 15°S and 15°N (Phillips et al., 2012; Humphrey et al., 2016). The combined driving effects of multiple TCs on TWS have also been reported regionally (De Linage et al., 2013; Räsänen and

* Corresponding author.
E-mail address: hebin@bnu.edu.cn (B. He).

https://doi.org/10.1016/j.jhydrol.2021.126419
Received 4 February 2021; Received in revised form 16 April 2021; Accepted 1 May 2021
Available online 8 May 2021

Kummu, 2013; Anyah et al., 2018), especially in the Northern Hemisphere (NH), where several climatic modes interact with each other within certain areas (Wang, 2004; Huang et al., 2017). However, a direct analysis of the effect of multiple TCs on TWS at the global scale is still missing, and the effective range of each TC and their mutual effect have hitherto not been fully identified to date. A comprehensive comparison of TC's impacts on global land water storage, including their spatial feedback pattern and relative contribution, is thus needed to guide their use in terrestrial water forecasting.

Here, we evaluate the climatic patterns expressed across global terrestrial water storage anomalies using observations from NASA's Gravity Recovery and Climate Experiment (GRACE) mission of the 14 major TC modes. We first describe the different influence spatial scales and correlation coefficients of TCs. Next, we illustrate the time lags of TWSA to each TC at global, regional and pixel scales. We then explore the terrestrial areas regulated by multiple TCs and identify the dominant TC for the given area. We also conduct time series analysis at the catchment scale to assess the phase change of multiple TCs and the TWSA response. Finally, we provide insight into the conceptual water balance framework by linking TC roles to precipitation, evapotranspiration and runoff and discuss limitations.

2. Data and methods

2.1. Teleconnections

TCs may refer to patterns arising from the internal variability of the atmosphere coupled with variations in the ocean. In this study, we analyze four globally important patterns of coupled atmosphere–ocean variability—the El Niño–Southern Oscillation(ENSO), the Pacific Decadal Oscillation (PDO), the Atlantic Multidecadal Oscillation (AMO), and the Indian Ocean Dipole (IOD)—and 10 additional climate patterns that dominate climate variability within the Northern and Southern Hemispheres. These regionally important TCs include the Arctic Oscillation (AO), Antarctic Oscillation (AAO), Pacific/North America (PNA), North Atlantic Oscillation (NAO), East Atlantic (EA), East Atlantic/Western Russia (EAWR), Polar/Eurasia (POL), Scandinavia (SCAND), West/Pacific (WP), and East Pacific-North Pacific (EPNP). Monthly data for the 14 teleconnection indices are obtained from the National Oceanic and Atmospheric Administration (NOAA). Here, we adopt the monthly multivariate ENSO index (MEI) for considering signals in both the atmosphere and the ocean, which has been shown to exhibit better behavior in correlating with TWS (Wolter and Timlin, 2011; Anyah et al., 2018). The PDO and AMO modes are defined as the leading surface temperature variability modes in the North Pacific and North Atlantic Ocean, respectively (MacDonald and Case, 2005; Ruprich-Robert and Cassou, 2014). Detailed information on all 14 TCs can be found in Supplementary Text S1.

2.2. GRACE data

From 2002 to 2017, the GRACE satellites measured monthly anomalies of the Earth's gravity field that can be used to obtain changes in terrestrial water storage. Here, we use the global monthly GRACE mass concentration (mascon) data at the spatial resolution of 0.5°produced by the Center for Space Research (CSR) at the University of Texas at Austin and NASA's Jet Propulsion Laboratory (JPL) to estimate the monthly TWS anomalies (TWSA). CSR mascon solutions are computed on an equal area geodesic pixel comprised of hexagonal tiles approximately 120 km wide (~1° at the equator) and are processed by constraining the original GRACE data through the Tikhonov regularization method, which effectively suppresses the north–south stripe errors in the GRACE measurements (Save et al., 2016). The JPL mascon data are calculated based on the equal area 3°×3° spherical cap mascon function and then use a priori constraints, including altimetry data and Global Land Data Assimilation System (GLDAS) land surface models (Rodell, 2004), to estimate the global gravity fields. These procedures can minimize the effect of measurement errors (Wiese et al., 2016). The coarse 3°×3° JPL mascon data is downscaled to 1°×1° using downscaling factors calculated with the Community Land Model 4.0 to reduce leakage errors introduced by the mascon basis function and finally resampled at 0.5°×0.5° grid cells (Scanlon et al., 2016; Watkins et al., 2015; Wiese et al., 2016). Detailed descriptions of the approaches used to process CSR and JPL Mascon products can be found in previous studies (Chambers and Bonin, 2012; Watkins et al., 2015; Save et al., 2016; Wiese et al., 2016).

We obtain the CSR mascon data and JPL mascon data from http://www.csr.utexas.edu/grace/RL05_mascons.htm and https://grace.jpl.nasa.gov/data/get-data/jpl_global_mascons/. Over land, we exclude the contribution of Greenland and Antarctica to obtain the monthly TWSA signal from Jan. 2003 to Dec. 2016. Missing records for 19 months are reconstructed using spline interpolation. Average values of GRACE-CSR-RL05 and GRACE-JPL are adopted to represent the GRACE observed TWSA, and the data series of GRACE-CSR-RL05, GRACE-JPL, GRACE-CSR-RL06 are used as reference information (Supplementary Figs. S6-S15). Because the focus of this study is on correlations between TWSA and climate variables, we subtract the seasonal cycle signals, the long-term trend and the semiannual signals in each TWSA time series using simple linear regression (Anyah et al., 2018; Humphrey et al., 2018). Considering that the 14-yr GRACE observation record cannot provide the decadal fluctuation of TWSA, we also use prolonged $TWSA_{\text{-rec}}$ data (1982–2016, dx.doi.org/https://doi.org//10.3929/ethz-b-000265949) simulated by GLDAS and trained by GRACE observations to confirm the correlations between TWSA and some long-period climate variability modes, such as AMO (Humphrey et al., 2018; Rodell, 2004).

2.3. Precipitation, evapotranspiration and runoff

The global 0.5° scale monthly precipitation datasets used in the study are obtained from the Climate Research Unit (CRU) Time Series 4.03 dataset (http://data.ceda.ac.uk//badc/cru/) and the Global Precipitation Climatology Centre (GPCC) (https://www.esrl.noaa.gov/psd/data/gridded/data.gpcc.html). GPCC precipitation data are used as reference information (Supplementary Figs. S16). Global datasets of terrestrial evapotranspiration are sourced from the European Centre for Medium-Range Weather Forecasts (ECMWF) ERA-Interim reanalysis dataset. Global monthly gridded basin-integrated observation-based runoff datasets based on the observed surface runoff values are collected from the Global Runoff Data Centre (GRDC: https://www.bafg.de/GRDC/EN/Home/homepage_node.html), and the missing data are simulated by a random forest model. Because these datasets have different spatial resolutions from the GRACE dataset, they are all converted to the same spatial resolution as 0.5°. The selection criteria for the investigated river basins are as follows: 1) river basin catchment area > 40,000 km^2, and 2) basin radius > 200 km (Scanlon et al., 2016) for the larger uncertainty of GRACE solution products within small river basins. Based on these criteria, 225 river catchments are chosen from the GRDC (Supplementary Table S1). Finally, both seasonal circle and long-term trends of precipitation, evapotranspiration and runoff data are removed by a method similar to the TWSA data processing.

2.4. Methods

Pearson's correlation analysis is used to explore the relationship between the detrending time series of TWSA and TCs at global, regional, pixel and catchment scales. The significance of correlations is evaluated at $p < 0.01$. To account for interferences arising from interactions between different climate phenomena, a partial least squares regression (PLS) model is implemented to disentangle the influence of different TCs on each other by considering interdependent and cross-correlated processes (Supplementary Fig. S17 and Text S2). Previous studies have indicated that climatic modes can lead to changes in hydrological variables over months and between seasons (Miralles et al., 2014; Sagarika et al., 2016; Vásquez et al., 2017). To account for the unknown response time of TWSA to climate variables, time lags ranging from 0 (i.e., no lag) to 12 months are introduced to each of the TCs during the calculation, resulting in 182 predictive features in total (i.e., 14 TCs × 13 lags per TC) (Martens et al., 2018).

3. Results

3.1. Global and regional TWSA response to climatic modes

We first calculate the correlations between TWSA and TCs with 0–12 months time lags (TWSA after TCs) at global and hemispheric scales (Fig. 1 and Supplementary Fig. S1). Then, we divide the global terrestrial area into 11 subregions according to the definitions of the Atmospheric Tracer Transport Model Intercomparison Project (TransCom) v3 (Gurney et al., 2003) as follows: Boreal North America, Temperate North America, Europe, Boreal Asia, Temperate Asia, Tropical South America, Temperate South America, North Africa, South Africa, Tropical Asia, and Australia. We then investigate the correlations between TWSA and TCs at the regional scale (Fig. 1a, 1b). Finally, we check the correlations between TWSA and TCs at the pixel level to draw detailed spatial response patterns (Fig. 1c). To avoid the possibility of false signals as much as possible, we only exhibit those results with statistically significant correlation coefficients ($p < 0.01$) and persistent relationships (significant correlation can be observed for three consecutive months).

Global TWSAs are found to be most strongly correlated with ENSO (r = −0.57), AMO (r = 0.47) and PDO (r = −0.37), followed by AO (r = −0.33), IOD (r = −0.32), EPNP (r = −0.22) and NAO (r = −0.27) (Fig. 1b and Supplementary Fig. S1). However, at the hemispheric scale, only ENSO, PDO and AMO exhibit a significant relationship with TWSA in both the Northern Hemisphere (NH, r as 0.37, 0.32 and 0.40, respectively) and Southern Hemisphere (SH, r as −0.63, −0.52 and −0.38, respectively). In contrast, IOD (r = −0.23) and AO (r = −0.23) are only significantly correlated with TWSA in NH, and NAO (r = -0.28) and EPNP (r = -0.26) are only correlated with TWSA in SH, demonstrating that they influence global TWSA via regulating special hemisphere's hydrological cycle. The other 6 TCs, including AAO, EA, PNA, POL, SCAND, and WP, show no significant correlation with TWSA at either the global or hemisphere scale, indicating their limited influence range. We also observed statistically significant correlations between TWSA and EAWR on global and hemisphere scales (r = -0.28, Supplementary Fig. S1). However, the subsequent regional and pixel analyses demonstrate that EAWR only affects TWSA in limited areas (2 subregions and 12.1% pixels, Fig. 1b, 1c); thus, its global effect is not discussed here.

Regional- and pixel-scale results indicate the global reach of ENSO, PDO and AMO on TWSA, with significant correlations being observed in

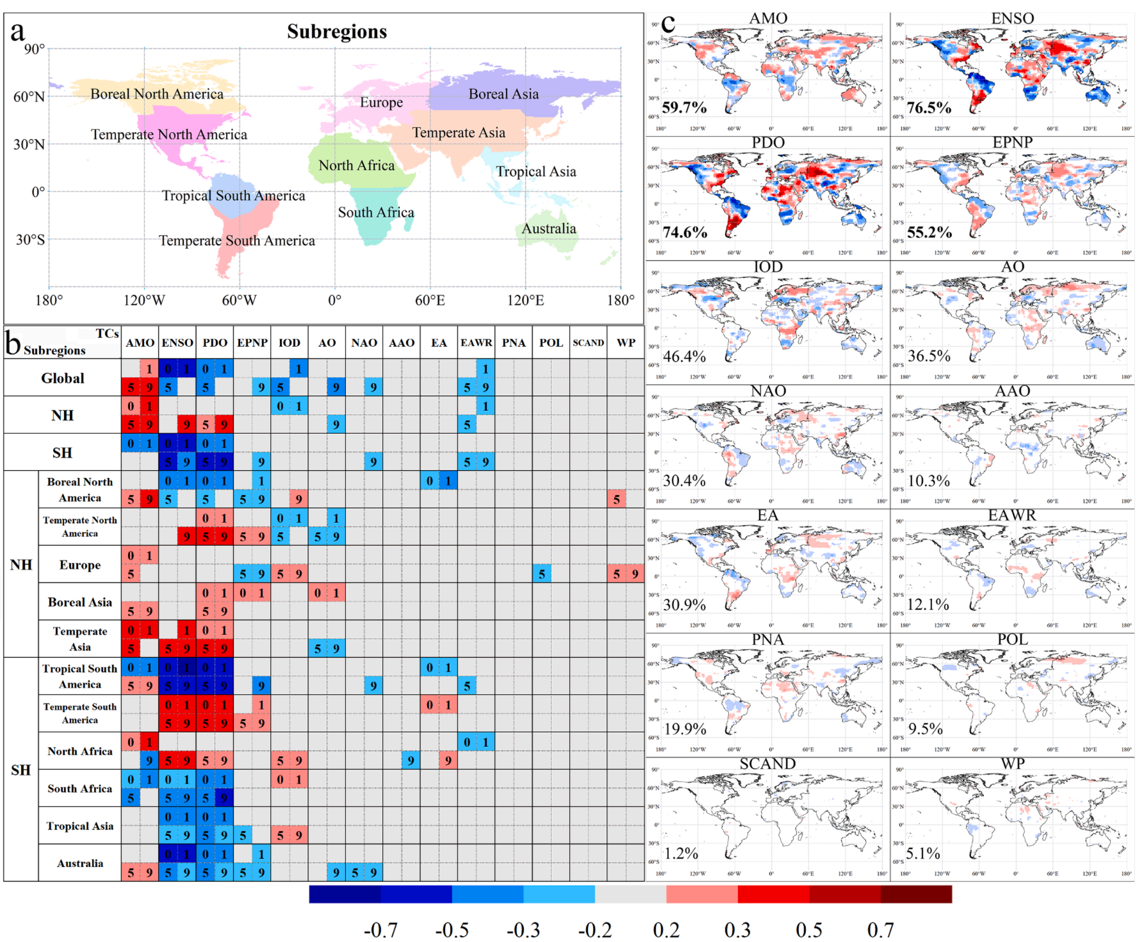

Fig. 1. **(a)** Division of the global terrestrial area into 11 subregions according to the definition used by TransCom v3. **(b)** Relationships between TCs and the average TWSA at global, hemispheric and regional scales. Each table row and column are labeled with region names and TC, respectively. The color of the grid cell indicates the greatest correlation coefficient among all lag times. Colored grids indicate that the maximum correlation coefficients pass the significance test. The numbers in the grids indicate the lag time of TWSA relative to variation in TCs: 0 refers to no time lag time during calculation, 1 refers to a 1–4 months lag of TWSA after TCs, 5 refers to a 5–8 months lag of TWSA after TCs, and 9 refers to a 9–12 month lag of TWSA after TCs. **(c)** Spatial pattern of correlation coefficients between TCs and average TWSA. Pixels showing with non-significant relationships ($p > 0.01$) are masked (i.e. blank area).

9 of all 11 subregions (over 76.5% pixels), 10 subregions (over 74.6% pixels), and 8 subregions (over 59.7% pixels) of global land (Fig. 1b and 1c). We support the previously reported strong negative correlations between TWSA and ENSO in tropical regions and SH (Phillips et al., 2012). As a replenishment, we find that TWSA and ENSO present significantly positive correlations in temperate regions (i.e., Temperate North America, Temperate Asia, Temperate South America and North Africa, Fig. 1b and 1c). Moreover, we observe the PDO's widespread influence on TWSA and similar spatial correlation pattern with ENSO, supporting the PDO's similar spatial range as ENSO in driving climate variables (Diaz et al., 2001; Gonsamo et al., 2016; Zhu et al., 2017). The EPNP is associated with the location and intensification shift of the Pacific jet stream from eastern Asia to the eastern North Pacific, and linked to surface temperature fluctuations over the North Pacific (Bell and Janowiak, 1995). Our results show that EPNP shares a similar but narrower spatial correlation pattern compared with ENSO and PDO, with significant correlations existing in 8 subregions (over 55.2% pixels). The observed wide effects of ENSO, PDO and EPNP on the TWSA strongly indicate the important role of the Pacific Ocean state in shaping the global terrestrial water cycle and suggest a cognate relationship among the three TCs.

With the short TWSA observation data (14 yrs), it is difficult to ascertain a reliable relationship with the multiple-decadal index such as AMO. The contemporary result shows that AMO is also the most important TC that strongly correlates with water storage in the majority of global land (8 subregions, over 59.7% pixels). We likewise noted that coefficients between AMO and TWSA increased as lag times increased (Supplementary Fig S15), suggesting its more long-lasting effects on TWS fluctuation.

Furthermore, simulated TWSA-rec data (1982–2016) show stronger regulation from AMO existing in wider regions (over 79.3%) than GRACE-observed TWSA (Supplementary Figs. S2 and S3).

IOD is associated with significant temperature and rain variability in the Indian Ocean rim regions (Ashok and Saji, 2007; Saji and Yamagata, 2003), and here, we identify IOD's effect on TWSA widely existing in 6 subregions (over 46.4% pixels), including boreal and temperate North America, Europe, Tropical Asia and North and South Africa. AO, AAO and NAO are reported to dominate the climate variations in the mid-high latitudes (Chen, 2014), while we find that AAO is correlated to the TWSA mainly in North Africa of SH (1 subregion, over 10.3% pixels globally). In contrast, AO and NAO affect TWSA in both hemispheres (4 subregions, over 36.5% pixels and 2 subregions, 30.4% pixels, respectively). Our results support the argument that AO and AAO are hardly taken as the distinct modes for they are usually combined with other TCs, and the teleconnection of AO is possibly the coexistence of NAO (Deser, 2000; Chen, 2014). The correlations between TWSA and the other 6 TCs (e.g., PNA, EA, EAWR, POL, SCAND and WP) are e relatively weak ($|r| \leq 0.35$) and regionally limited, indicating their relatively minor impact on global land water regulation.

3.2. The differentiate contributions of TCs to TWSA

By examining the relationships among TWSA and 14 TCs at the pixel scale, we find that TWSA is significantly correlated with one or more of the studied TCs in over 97.5% of the global land area (Fig. 2a), indicating the potential forecasting ability of multiple TCs on global land water resources. The correlation map shows that regions with the most significant correlation coefficients are consist with the drainage area of major river basins (e.g., the Orinoco river basin, Zambezi river basin, Mackenzie river basin and OB river basin). This observation supports previous findings that river basins exhibit clearer climate signals than other area by collecting and consolidating rainwater over a large catchment (Phillips et al., 2012). Furthermore, our results show that the TWSA in over 91.8% of the terrestrial areas is correlated with multiple TCs (over three TCs). Among these, the TWSA in over 19.9% of areas is significantly correlated with over 7 TCs (Fig. 2b), which are mainly distributed in subregions such as Boreal North America, Tropical South America and North Africa (Fig. 1b). Regions with TWSA responses to 5–6 TCs cover 41.8% of the global land area and are mainly distributed in subregions such as Temperate North America, Europe and Australia. The complex pattern of TC effects on TWSA observed here highlights the necessity to investigate the combined effects of multiple TCs rather than

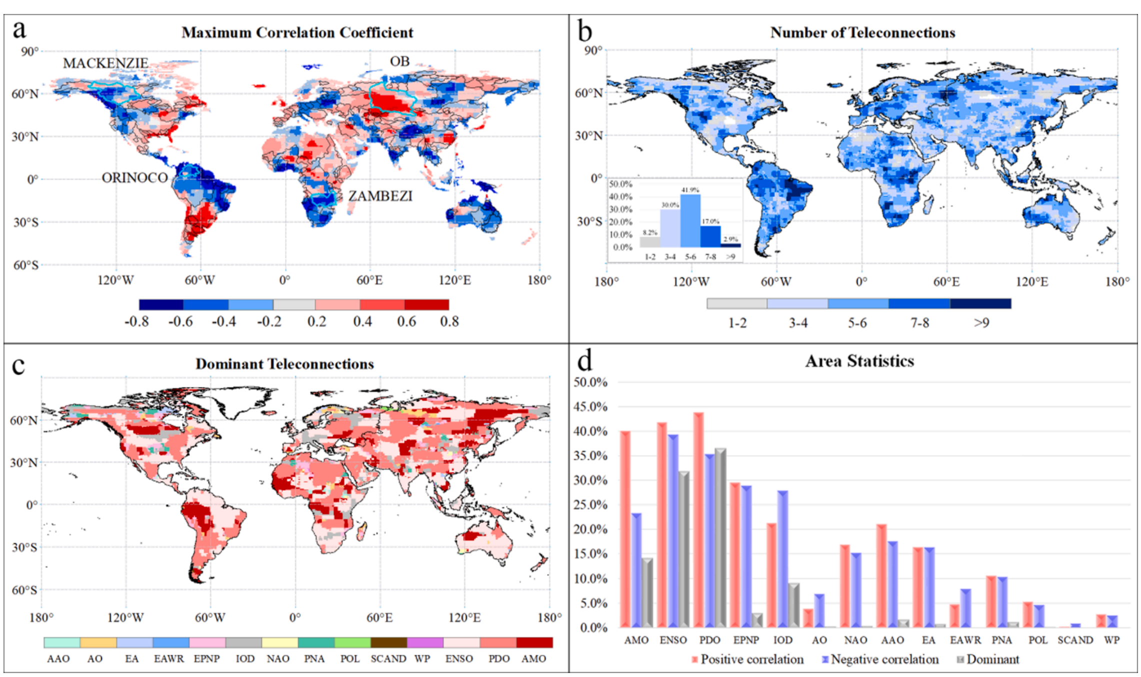

Fig. 2. The different contributions of various TCs to the local TWSA for the period 2003–2016. (a) Maps of the investigated regions color-coded based on the value of the maximum correlation coefficient found between TWSA and TCs. (b) Maps of investigated regions color-coded based on the numbers of TCs significantly correlated with local TWSA. (c) Maps of the investigated regions color-coded according to the identity of the TCs-dominated local TWSA. (d) The percentage of the global land surface significantly correlated and dominated by each TC and color-coded based on their correlated coefficients.

try to link large-scale hemispheric climate and hydrological variability to the single climatic mode.

To disentangle the contributions of each TC, we conduct the partial least squares regression (PLS) model by considering the interdependent and cross-correlated processes considering 0–12 months time lags. The TC with the maximum regression coefficient of each pixel is defined as the dominant TC of the pixel (Fig. 2c), and the corresponding lag time is defined as the optimal lag of this dominant teleconnection (Supplementary Fig. S4). The TWSA in over 91.9% of terrestrial pixels is dominated by 4 global TCs: PDO (36.6%), ENSO (31.8%), AMO (14.3%) and IOD (9.2%) (Fig. 2d). Compared to its widest impacting area and strong correlations, we find that ENSO dominates TWSA in limited areas, predominantly distributed in tropical regions, the northern part of Africa and Australia, and scattered regions in NH (Fig. 2c). In contrast, the PDO is identified as the climate mode that dominates the TWSA in the widest area, including the central Asia, the North Africa and the southern part of South America, corresponding to the PDO's robust relationships with dry/wet conditions in these regions (Sun et al., 2016). The AMO is always the most important TC in affecting the TWSA in the western Amazon Basin and Siberian region. The observed presence of IOD-dominated TWSA is noticeable in the tropical Indian Ocean rim regions and scattered in North America and Western Europe, substantially consistent with the reported remotely affected regions of IOD (Saji and Yamagata, 2003), except for Australia without signals in this study. While the spatial distribution of the lag time is fragmented (Supplementary Fig. S4), the lag times of TWSA in the ENSO-dominated area are generally shorter (average 4.3 months) than those of PDO (average 5.3 months), AMO (average 6.4 months) and IOD (average 6.2 months), suggesting the relative faster response of TWSA to ENSO.

3.3. Coordinated variations in multiple TCs at the catchment scale.

To further investigate the multiple TC interaction process, we evaluate the effect of TCs on TWSA at the catchment scale. Then we conduct time-series processing to check the coordinated variations of multiple TCs in two selected river basins. The correlation map shows regions with the most significant correlation coefficient following the drainage area of major river basins (Fig. 2a and Fig. 3a). This observation supports previous findings that river basins exhibit clearer climate signals than other areas by collecting and consolidating rainwater over a large catchment (Phillips et al., 2012). Catchments with weak correlations between TWSA and TCs are concentrated in Central Africa (the Nile River basin), central Asia (the Yenisei River basin and Amur basin), Western North America (the Yukon basin) and Eastern Siberia (the Kolyma River basin) (Fig. 3a), suggesting that other factors, including other climate mechanisms or anthropogenic activities, dominate changes of TWSA there.

Corresponding with the results at the pixel and regional scales, we observe that the TWSA of most river basins is affected by multiple TCs (Supplementary Table S1). The synergistic effect of multiple TCs can

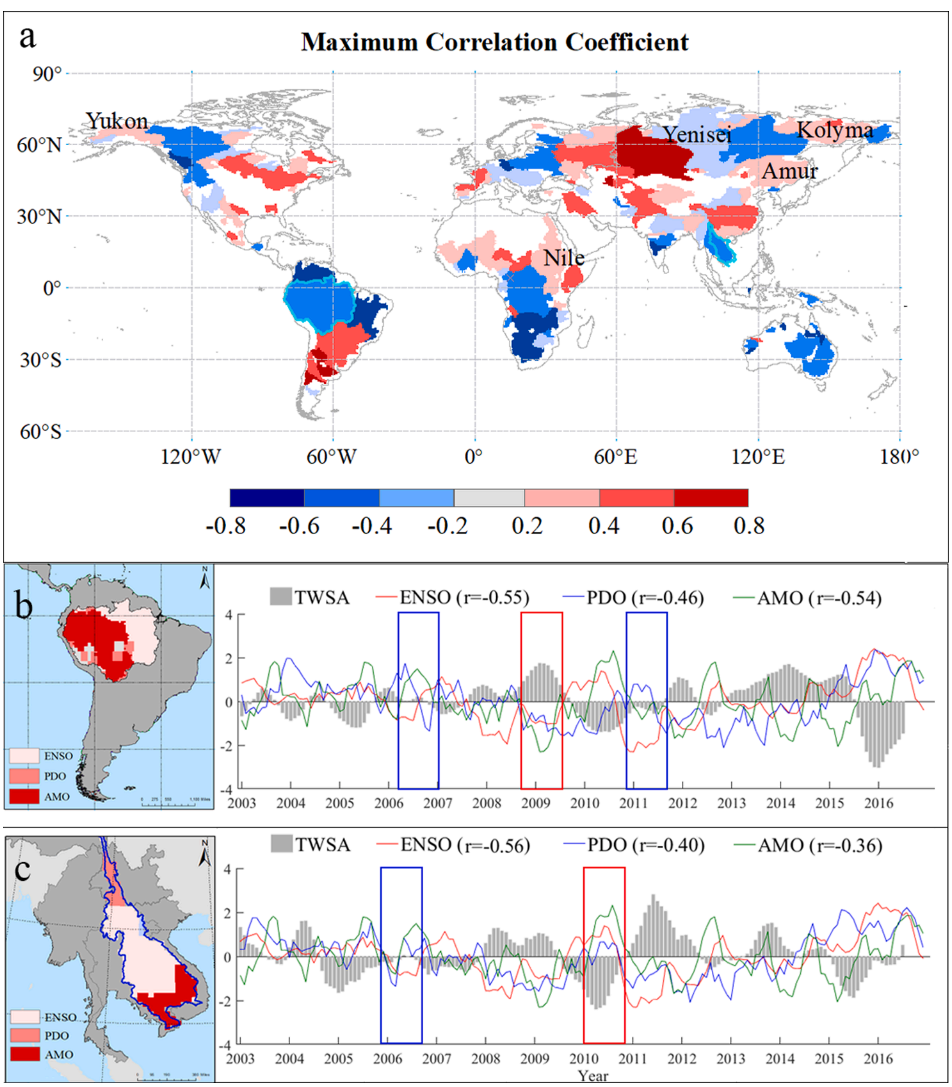

Fig. 3. The response of TWSA to multiple TCs within investigated water catchments. (a) Maps of the investigated water catchments color-coded based on the value of the maximum correlation coefficient found between TWSA and TCs. (b) Time series of TWSA and correlated TCs in the Amazon basin (top) and Mekong River basin (bottom). Red boxes plot the phase synchronization cases of three TCs, and blue boxes plot the non-synchronization cases. (For interpretation of the references to color in this figure legend, the reader is referred to the web version of this article.)

also be observed in previously confirmed sensitive catchments to ENSO, such as the Amazon River basin (Marengo et al., 2011; Phillips et al., 2012; Gloor et al., 2015). The time curves show that the TWSA in the Amazon Basin is most sensitive to the synchronous fluctuations of ENSO, PDO and AMO (Fig. 3b). The synchronous negative phase of PDO, ENSO and AMO usually leads to a stronger positive TWSA, and vice versa (labeled as red boxes in Fig. 3b). In contrast, incongruent phases of the three TCs will serve to cancel out and weaken each other, leading to weaker TWSA (labeled as blue boxes). Previous reports have indicated that a positive PDO phase is associated with an increase in precipitation in the southern Amazon and higher eastern Pacific temperatures over most of the Amazon River basin (Gloor et al., 2015), Positive ENSO alters wind patterns and contributes to positive precipitation anomalies (Van Oldenborgh and Burgers, 2005; Marengo et al., 2011). The combined effects of PDO and ENSO intensify the Walker circulation characterized by an increase in air upwelling and precipitation over the Amazon basin (McGregor et al., 2014). Meanwhile, AMO indirectly affects TWSA by modulating the intensity of the ENSO cycle (Vásquez et al., 2017) and commonly contributes to the greater fluctuations of TWSA. Similar conditions can also be clearly observed in the Mekong River basin (Räsänen and Kummu, 2013; Saji and Yamagata, 2003).

4. Discussion

4.1. Combined effect of multiple TCs on TWSA

Many modes of climate variability are considered potential drivers of hydrological variability (Phillips et al., 2012; McGregor, 2017; Martens et al., 2018). After conducting a joint evaluation on global, regional and catchment scales, we prove the widespread impact of TCs on TWSA, with significant correlations observed in over 97.5% of the global terrestrial grid area. This demonstrates that water storage in most global land surfaces is regulated by remote ocean–atmosphere states and supports the strong predictive ability of the TC index. In addition to previously reported sensitive regions of the TWSA, such as tropical regions and the SH (Phillips et al., 2012; Anyah et al., 2018), the middle and high latitudes of the NH are also identifiedas sensitive TC-impacting areas.

Among all studied TCs, ENSO affects TWSA dynamics in the largest portion of land (76.5%), confirming that ENSO is the most important mode as reported (Van Oldenborgh and Burgers, 2005; Marengo et al., 2011; Phillips et al., 2012). However, several teleconnections, e.g., PDO (74.6%), AMO (59.7%) and IOD (46.4%), affect TWSA over extensive areas. ENSO, PDO and AMO have been previously reported to be the dominant climatic modes driving global carbon fluxes (Gonsamo et al., 2016; Zhu et al., 2017). Our findings suggest that the effects of TCs on the terrestrial carbon cycle may be at least partly driven by their effects on terrestrial water storage, since changes in TWS have been reported to strongly affect the terrestrial carbon sink at global and continental scales (Humphery, et al., 2018). ENSO is found to dominate TWSA in only 31.8% of its effect region, in agreement with the findings of Marten et al. (2018) that the global effects of ENSO on climate are generally subordinate to the effects of other TCs within the specific geographic area. Regional climate modes, such as AO, EA and EAWR, are reported to affect terrestrial water distribution by controlling the atmospheric circulation of specific regions (Bell and Janowiak, 1995; Silvestri and Vera, 2003; Overland and Wang, 2005; Gao et al., 2016). There is potential for predicting atmosphere–ocean state-induced global land water storage anomalies by assimilating multiple climatic modes.

An impressive finding is that fluctuations in water storage are regulated by multiple climatic modes in over 91.9% of the global land area, and TWSA in over 61.8% of the area is impacted by over 5 TCs. This suggests that terrestrial water resource forecasting models that adopt single or limited TC indices can hardly capture signals from ocean and atmospheric states. Furthermore, we reveal that TWSAs are sensitive to coordinated variations in multiple TCs. After examining 168-months-long records from the Amazon and Mekong River basins, we find that the maximum (minimum) values of TWSA frequency coincided with the signals stack in the same phase. Correspondingly, the out-of-phase combination of multiple TCs is inclined to weaken their impact on TWSA. Low-frequency cycles, such as the AMO and PDO, are reported to modulate high-frequency cycles such as ENSO, contributing to the enhanced or dampened ENSO-hydrology relationship in interdecadal periods (Hallett et al., 2004; Gonsamo et al., 2016; McGregor, 2017). Since the relationship between TCs and TWSA is likely to be dynamic and the different TC combinations exist over regions (Phillips, et al., 2012; Forootan et al., 2016), we prove that the phase combination of local correlated climatic modes would shift land hydrological response behaviors. How the climatic modes at various temporal scales interact is not yet adequately understood, and the varied coupling between TCs and TWSA at longer historical time scales calls for further studies.

4.2. TCs regulating TWSA via water budget processes

TC modes regulate the global terrestrial water cycle by mediating precipitation (P), evapotranspiration (ET), runoff (R) and glacial melting in the cryosphere (Long, et al., 2014; Resende et al., 2018). To further track TC's impact on terrestrial water cycles, we bridge TC impacts on each hydrological component based on the land water budget equation in each river basin. First, we calculate the contributions of P, ET, and R to the TWSA in each catchment and then check each TC's contributions to P, ET and R via PLS models (Fig. 4, Supplementary Fig. S5).

We find that the TWSAs of 51 river basins (covering over 40.6% of the studied catchment areas) are predominantly driven by precipitation (contribution $> 50\%$), and mainly located in the mid-latitude 30° or above of both hemispheres. ENSO and EPNP are the dominant TCs driving P fluctuations in these river basins. This finding supports previous reports that ENSO and EPNP reflect the total volume of water vapor moving from the tropical ocean to the inner land (Wang, 2004; Van Oldenborgh and Burgers, 2005; Emerton et al., 2017) and in turn regulate the water storage of the inner land. Moreover, water storage in the river basins located in the high-latitude and high-elevation regions is partly replenished by melting snow or glaciers (Emerton et al., 2017; Martens, et al., 2018). Considering the neglected impacts of TCs on TWSA via the temperature-induced melting process, the contributions of TCs to TWSA in high latitude regions are probably underestimated (Hirschi et al., 2006; Syed et al., 2009; Zhang et al., 2019).

Totally 130 river basins (covering over 51.1% of the studied catchment areas) are found whose water storage is controlled by ET, and mainly distributed in tropical and subtropical regions. Water availability is not limited in these regions, and climatic modes affect terrestrial evaporation by altering the atmospheric demand for water (Martens et al., 2018). The broad area of water temperature anomalies and changes in the trade winds along the equator are classic features of the ENSO, which may lead to associated changes in ET within tropical and subtropical regions (Miralles et al., 2014). TWSAs in 6 river basins (covering 2.7% of total areas) are observed to be driven by R in this study. The relations between stream flow and modes of climate variability in the catchment are reported to be non-monotonic and associated with catchment characteristics such as glaciation (Fleming and Dahlke, 2014).

It is worth noting that the relationship between TCs and TWSA is likely to be dynamic. There is evidence that teleconnection patterns may shift their climate driving mechanism during different phases and lead to different impacts on hydrological components (Miralles et al., 2014; Ruprich-Robert and Cassou, 2014; Fang et al., 2017; McGregor, 2017). Moreover, the integration of these hydrological components over time could generate additional uncertainty in the TWSA, such as the positive precipitation led by the combined effects of multiple TCs often being tied to extra runoff resulting from floods (Emerton et al., 2017; McGregor, 2017).

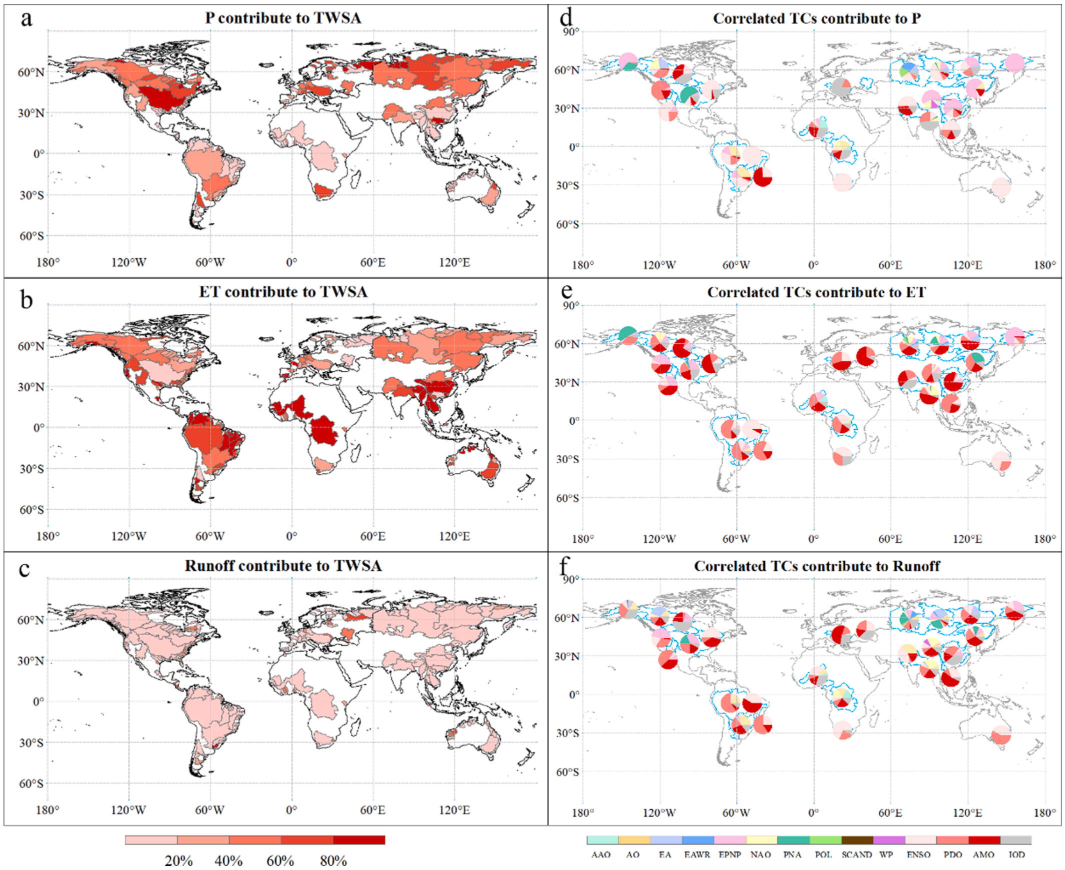

Fig. 4. Maps of variations in TWSA contributed from (a) precipitation (P), (b) evapotranspiration (ET) and (c) runoff (R) and spatial patterns of variations in (d) precipitation (P), (e) evapotranspiration (ET) and (f) runoff (R) contributed from multiple TCs (color-coded) of the investigated river basins. Only part of the calculated contribution results is shown here for the limitation of exhibition space, and the full results can be found in Table S1.

5. Conclusions

To achieve a comprehensive understanding of multiple TCs' effects on hydrological activity, we present here a global framework on correlations with terrestrial hydrological processes and associated ocean/atmosphere states. Despite the uncertainties mentioned above, our study observes that the TWSA is sensitive to one or more of these climatic TCs over 97.5% of the global terrestrial area. We report the robust effects of ENSO, PDO and AMO on driving variations in TWSA, demonstrated by wide areas of effect and strong correlations that persisted for several months at the global, hemisphere, continent and catchment scales. Moreover, the TWSA in over 91.8% of the terrestrial area (62.2% of water basins) is regulated by multiple TCs and sensitive to coordinated variations of multiple TCs.

ENSO, PDO, AMO and IOD are identified as the most important modes which dominate TWSA in most of the global land surface. Considering the integrated correlation of multiple TCs on TWSA, ENSO is not the most important TC in mediating TWSA. The PDO is observed to dominate the TWSA in 36.6% of the global area, compared to 31.8% of ENSO. Regional climatic modes, such as AO, EA, EAWR and NAO, are also found to dominate the TWSA in specific areas. The climatic modes generally exert a comprehensive but not equally important impact on land hydrological components and are finally exhibited in variations in land water storage. We note that some confounding factors, such as human-induced activities, including land use change and river regulation, are not discussed in this study. These factors can certainly influence TWSA changes but are not necessarily related to climatic TCs.

CRediT authorship contribution statement

Lanlan Guo: Conceptualization, Writing - original draft. **TieWei Li:** Methodology, Formal analysis, Investigation, Data curation, Visualization. **Deliang Chen:** . **Junguo Liu:** . **Bin He:** Conceptualization. **Yafeng Zhang:** .

Declaration of Competing Interest

The authors declare that they have no known competing financial interests or personal relationships that could have appeared to influence the work reported in this paper.

Acknowledgments

This work is financially supported by the Strategic Priority Research Program of Chinese Academy of Sciences (Grant No. XDA20060402), National key research and development program (Grant No. 2018YFC1509003), Swedish STINT (Grant No. CH2015-6226), and the Swedish VR (Grant No. 2017-03780).

Appendix A. Supplementary data

Supplementary data to this article can be found online at https://doi.org/10.1016/j.jhydrol.2021.126419.

References

Anyah, R.O., Forootan, E., Awange, J.L., Khaki, M., 2018. Understanding linkages between global climate indices and terrestrial water storage changes over Africa using GRACE products. Sci. Total Environ. 635, 1405–1416.

Ashok, K., Saji, N.H., 2007. On the impacts of ENSO and Indian Ocean dipole events on subregional Indian summer monsoon rainfall. Nat. Hazards 42 (2), 273–285.

Bell, G.D., Janowiak, J.E., 1995. Atmospheric circulation associated with the Midwest floods of 1993. Bull. Am. Meteorol. Soc. 76 (5), 681–695.

Chambers, D.P., Bonin, J.A., 2012. Evaluation of Release-05 GRACE time-variable gravity coefficients over the ocean. Ocean Sci. 8 (5), 859–868.

Chen, G.e., 2014. Revisit to atmospheric oscillations over global oceans: a combined climatology/modality approach. Int. J. Climatol. 34 (8), 2715–2729.

de Linage, C., Kim, H., Famiglietti, J.S., Yu, J.-Y., 2013. Impact of pacific and atlantic sea surface temperatures on interannual and decadal variations of grace land water storage in tropical south America. J. Geophys. Res. Atmosph. 118 (19), 10,811–10,829.

Deser, C., 2000. On the teleconnectivity of the "Arctic Oscillation". Geophys. Res. Lett. 27, 779–782.

Diaz, H.F., Hoerling, M.P., Eischeid, J.K., 2001. ENSO variability, teleconnections and climate change. Int. J. Climatol. 21 (15), 1845–1862.

Emerton, R., Cloke, H.L., Stephens, E.M., Zsoter, E., Woolnough, S.J., Pappenberger, F., 2017. Complex picture for likelihood of ENSO-driven flood hazard. Nat. Commun. 8, 1–9.

Fang, Y., Michalak, A.M., Schwalm, C.R., Huntzinger, D.N., Berry, J.A., Ciais, P., Piao, S., Poulter, B., Fisher, J.B., Cook, R.B., Hayes, D., Huang, M., Ito, A., Jain, A., Lei, H., Lu, C., Mao, J., Parazoo, N.C., Peng, S., Ricciuto, D.M., Shi, X., Tao, B.o., Tian, H., Wang, W., Wei, Y., Yang, J., 2017. Global land carbon sink response to temperature and precipitation varies with ENSO phase. Environ. Res. Lett. 12 (6), 064007. https://doi.org/10.1088/1748-9326/aa6e8e.

Feng, T., Wigneron, J.-P., Ciais, P., Chave, J., Ogée, J., Peñuelas, J., Ræbild, A., Domec, J.-C., Tong, X., Brandt, M., Mialon, A., Rodriguez-Fernandez, N., Tagesson, T., Al-Yaari, A., Kerr, Y., Chen, C., Myneni, R.B., Zhang, W., Ardö, J., Fensholt, R., 2018. Coupling of ecosystem-scale plant water storage and leaf phenology observed by satellite. Nat. Ecol. Evol. 2 (9), 1428–1435.

Fleming, S. W. and Dahlke, H. E. (2014) Parabolic northern hemisphere river flow teleconnections to El Nin õ- Southern Oscillation and the Arctic Oscillation. Environ. Res. Lett., 9, Article Number: 104007.

Forootan, E., Safari, A., Mostafaie, A., Schumacher, M., Delavar, M., Awange, J.L., 2017. Large-scale total water storage and water flux changes over the arid and semiarid parts of the middle east from grace and reanalysis products. Surv. Geophys. 38 (3), 591–615.

Forootan, E., Kusche, J., Loth, I., Schuh, W.-D., Eicker, A., Awange, J., Longuevergne, L., Diekkrüger, B., Schmidt, M., Shum, C.K., 2014. Multivariate Prediction of Total Water Storage Changes Over West Africa from Multi-Satellite Data. Surv. Geophys. 35 (4), 913–940.

Gao, T., Yu, J.Y., Paek, H., 2016. Impacts of four northern-hemisphere teleconnection patterns on atmospheric circulations over Eurasia and the Pacific. Theor. Appl. Climatol. 129 (3–4), 815–831.

Gloor, M., Barichivich, J., Ziv, G., Brienen, R., Schöngart, J., Peylin, P., Ladvocat Cintra, B.B., Feldpausch, T., Phillips, O., Baker, J., 2015. Recent Amazon climate as background for possible ongoing and future changes of amazon humid forests. Global Biogeochem. Cycles 29 (9), 1384–1399.

Gonsamo, A., Chen, J.M., Lombardozzi, D., 2016. Global vegetation productivity response to climate oscillations during the satellite era. Glob. Change Biol. 22 (10), 3414–3426.

Gurney, K.R., Law, R.M., Denning, A.S., Rayner, P.J., Baker, D., Bousquet, P., et al., 2003. TransCom 3 CO_2 inversion intercomparison: 1. annual mean control results and sensitivity to transport and prior flux information. Tellus Ser. B-chem. Phys. Meteorol. 55 (2), 555–579.

Hallett, T.B., Coulson, T., Pilkington, J.G., Cluttonbrock, T.H., Pemberton, J.M., Grenfell, B.T., 2004. Why large-scale climate indices seem to predict ecological processes better than local weather. Nature 430 (6995), 71–75.

Hirschi, M., Seneviratne, S.I., Schär, C., 2006. Seasonal variations in terrestrial water storage for major midlatitude river basins. J. Hydrometeorol. 7 (1), 39–60.

Huang, W., Chen, R., Yang, Z., Wang, B., Ma, W., 2017. Exploring the combined effects of the Arctic Oscillation and ENSO on the wintertime climate over east Asia using self-organizing maps. J. Geophys. Res. 122 (17), 9107–9129.

Humphrey, V., Gudmundsson, L., Seneviratne, S.I., 2016. Assessing global water storage variability from grace: trends, seasonal cycle, subseasonal anomalies and extremes. Surv. Geophys. 37 (2), 357–395.

Humphrey, V., Zscheischler, J., Ciais, P., Gudmundsson, L., Sitch, S., Seneviratne, S.I., 2018. Sensitivity of atmospheric CO_2 growth rate to observed changes in terrestrial water storage. Nature 560 (7720), 628–631.

Long, D.i., Longuevergne, L., Scanlon, B.R., 2014. Uncertainty in evapotranspiration from land surface modeling, remote sensing, and grace satellites. Water Resour. Res. 50 (2), 1131–1151.

MacDonald, G.M., Case, R.A., 2005. Variations in the Pacific Decadal Oscillation over the past millennium. Geophys. Res. Lett. 32 (8).

Marengo, J.A., Tomasella, J., Alves, L.M., Soares, W.R., Rodriguez, D.A., 2011. The drought of 2010 in the context of historical droughts in the Amazon region. Geophys. Res. Lett. 38 (12), n/a–n/a.

Martens, B., Waegeman, W., Dorigo, W.A., Verhoest, E.C.N., Miralles, G., 2018. Terrestrial evaporation response to modes of climate variability. npj Clim. Atmos. Sci. 1–43.

McGregor, G., 2017. Hydroclimatology, modes of climate variability and stream flow, lake and groundwater level variability: a progress report. Prog. Phys. Geogr. 41 (4), 496–512.

McGregor, S., Timmermann, A., Stuecker, M.F., England, M.H., Merrifield, M., Jin, F.-F., Chikamoto, Y., 2014. Recent Walker circulation strengthening and Pacific cooling amplified by Atlantic warming. Nat. Clim. Change 4 (10), 888–892.

Miralles, D.G., van den Berg, M.J., Gash, J.H., Parinussa, R.M., de Jeu, R.A.M., Beck, H. E., Holmes, T.R.H., Jiménez, C., Verhoest, N.E.C., Dorigo, W.A., Teuling, A.J., Johannes Dolman, A., 2014. El Niño–La Niña cycle and recent trends in continental evaporation. Nat. Clim. Change 4 (2), 122–126.

Overland, J.E., Wang, M., 2005. The Arctic climate paradox: The recent decrease of the Arctic Oscillation. Geophys. Res. Lett. 32 (6), 347–354.

Phillips, T., Nerem, R.S., Fox-Kemper, B., Famiglietti, J.S., Rajagopalan, B., 2012. The influence of ENSO on global terrestrial water storage using grace. Geophys. Res. Lett. 39 (16), n/a–n/a.

Räsänen, T.A., Kummu, M., 2013. Spatiotemporal influences of ENSO on precipitation and flood pulse in the Mekong River Basin. J. Hydrol. 476, 154–168.

Resende, T.C., Longuevergne, L., Gurdak, J.J., Leblanc, M., Favreau, G., Ansems, N., Aureli, A., 2018. Assessment of the impacts of climate variability on total water storage across Africa: implications for groundwater resources management. Hydrogeol. J. 1–20.

Rodell, M., 2004. Basin scale estimates of evapotranspiration using GRACE and other observations. Geophys. Res. Lett. 31 (20), L20504.

Ruprich-Robert, Y., Cassou, C., 2014. Combined influences of seasonal East Atlantic Pattern and North Atlantic Oscillation to excite Atlantic multidecadal variability in a climate model. Clim. Dyn. 44 (1–2), 229–253.

Sagarika, S., Kalra, A., Ahmad, S., 2016. Pacific Ocean SST and Z500 climate variability and western US seasonal streamflow. J. Climatol. 36 (3), 1515–1533.

Save, H., Bettadpur, S., Tapley, B.D., 2016. High-resolution CSR GRACE RL05 mascons. J. Geophys. Res. Solid Earth 121 (10), 7547–7569.

Saji, N., Yamagata, T., 2003. Possible impacts of Indian Ocean dipole mode events on global climate. Climate Research 25 (2), 151–169.

Scanlon, B.R., Zhang, Z., Save, H., Wiese, D.N., Landerer, F.W., Long, D.i., Longuevergne, L., Chen, J., 2016. Global evaluation of new GRACE mascon products for hydrologic applications. Water Resour. Res. 52 (12), 9412–9429.

Silvestri, G.E., Vera, C.S., 2003. Antarctic Oscillation signal on precipitation anomalies over southeastern South America. Geophys. Res. Lett. 30 (21), 1–4.

Sun, Q., Miao, C., AghaKouchak, A., Duan, Q., 2016. Century-scale causal relationships between global dry/wet conditions and the state of the Pacific and Atlantic oceans. Geophys. Res. Lett. 43 (12), 6528–6537.

Syed, T.H., Famiglietti, J.S., Chambers, D.P., 2009. GRACE-based estimates of terrestrial freshwater discharge from basin to continental scales. J. Hydrometeorol. 10 (1), 22–40.

Van Oldenborgh, G.J., Burgers, G., 2005. Searching for decadal variations in ENSO precipitation teleconnections. Geophys. Res. Lett. 32 (15).

Vásquez, P.I.L., Nascimento de Araujo, L.M., et al., 2017. Historical analysis of interannual rainfall variability and trends in southeastern Brazil based on observational and remotely sensed data. Clim. Dyn. 50 (3–4), 801–824.

Wang, C. (2004). ENSO, Atlantic Climate Variability, and the Walker and Hadley Circulations. The Hadley Circulation: Present, Past and Future. Springer Netherlands, 30(21).

Watkins, Michael M., Wiese, David N., Yuan, Dah-Ning, Boening, Carmen, Landerer, Felix W., 2015. Improved methods for observing Earth's time variable mass distribution with GRACE using spherical cap mascons. J. Geophys. Res. Solid Earth 120 (4), 2648–2671.

Wiese, David N., Landerer, Felix W., Watkins, Michael M., 2016. Quantifying and reducing leakage errors in the JPL RL05M GRACE mascon solution. Water Resour. Res. 52 (9), 7490–7502.

Wolter, K., Timlin, M.S., 2011. El Niño/Southern Oscillation behaviour since 1871 as diagnosed in an extended multivariate ENSO index (MEI. ext). Int. J. Climatol. 31 (7), 1074–1087.

Zhang, Yafeng, He, Bin, Guo, Lanlan, Liu, Junjie, Xie, Xiaoming, 2019. The relative contributions of precipitation, evapotranspiration, and runoff to terrestrial water storage changes across 168 river basins. J. Hydrol. 579, 124194. https://doi.org/10.1016/j.jhydrol.2019.124194.

Zhu, Zaichun, Piao, Shilong, Xu, Yaoya, Bastos, Ana, Ciais, Philippe, Peng, Shushi, 2017. The effects of teleconnections on carbon fluxes of global terrestrial ecosystems. Geophys. Res. Lett. 44 (7), 3209–3218.